Journal of Solid State Chemistry 352 (2025) 125597

Contents lists available at ScienceDirect

Journal of Solid State Chemistry

journal homepage: www.elsevier.com/locate/jssc

Insights into the phase stability window, phase transformation behavior, and anisotropic thermal expansion of rhombohedral bismuth oxide

Mathias A. Kiefer [a,b], Caren Billing [a,b,*], Daniel Olds [c], David G. Billing [a,b]

[a] Molecular Science Institute, School of Chemistry, University of the Witwatersrand, Private Bag X3, Johannesburg, 2050, South Africa
[b] DSI-NRF Centre of Excellence in Strong Materials, University of the Witwatersrand, Private Bag X3, Johannesburg, 2050, South Africa
[c] National Synchrotron Light Source II, Brookhaven National Laboratory, PO Box 5000, Upton, NY, 11973, USA

ARTICLE INFO

Keywords:
Bismuth oxide
Rhombohedral phase
Phase stability
Thermal expansion
Phase transition

ABSTRACT

Rhombohedral bismuth oxide has emerged as a promising SOFC electrolyte material, particularly at low-to-intermediate temperatures. The stability window of this phase was explored using a co-doped system, using yttrium and lanthanum or aluminum, over 7.5–25 % total dopant content and 0.907–1.154 Å weighted average dopant cationic radius. The phase transformation behavior of rhombohedral-rich phase mixtures was also investigated *in situ* from 360 to 656 °C to assess the effects of minor impurity phases and thermal evolution pathways. Our results reveal that low-dopant, rhombohedral-rich compositions exhibit poor structural stability upon heating. Anisotropic thermal expansion behavior was observed over 450–656 °C, serving as a sensitive indicator of sequential phase changes, including the rhombohedral β_2-to-β_1 transition (~450 °C), monoclinic phase formation, and delayed or incomplete formation of the cubic phase (~ 550 °C). These multiple unfavorable phase transitions compromise the mechanical robustness required for SOFC operation. This study underscores the need for compositional tuning to balance ionic conductivity with thermal phase stability in rhombohedral Bi_2O_3-based systems.

1. Introduction

Bismuth oxide-based materials are known to crystallize in several polymorphs (Fig. 1), the formation of which is dependent on both composition and thermal treatment. In undoped Bi_2O_3, the stable phase at room temperature is the monoclinic α-phase ($P2_1/c$, SG #14 with unit cell volume ≈ 339 Å^3), which transforms to the tetragonal β-phase around 650 °C ($P4_2/nmc$, SG #137 with unit cell volume ≈ 328 Å^3), followed by a transition to the high-temperature cubic δ-phase above ~730 °C ($Fm\,\overline{3}\,m$, SG #225 with unit cell volume ≈ 180 Å^3) [1–5].The high oxide ion conductivity of the high temperature cubic δ-polymorph has resulted in this phase being extensively studied for application as a solid oxide fuel cell (SOFC) electrolyte [1–3]. Partially substituting Bi^{3+} with certain metal ions, including Y^{3+}, has successfully stabilized the δ-polymorph phase to room temperature, at minimal expense to the ionic conductivity. [6–13]. The existence of a rhombohedral phase ($R\,\overline{3}\,m$, SG #166 with unit cell volume ≈ 380 Å^3) in the Bi_2O_3–Y_2O_3 system was initially identified by Watanabe and Kikuchi [14]. This is an ionically conductive hexagonal phase isomorphous to rhombohedral compounds formed in alkali earth doped bismuth oxides and is not a natural polymorph of pure Bi_2O_3. This phase was later studied via Rietveld methods by Zhang et al. [12] and confirmed to crystallize in the rhombohedral $R\,\overline{3}\,m$ space group. The rhombohedral phase is often found when Bi^{3+} is partially substituted by large cations, such as La^{3+} [15–17].

Several studies have characterized the ionic conductivity of rhombohedral bismuth oxides, often reporting favorable transport properties at low to intermediate temperatures (400–700 °C) which exceed that of the δ-phase [16–19]. However, ionic conductivity was found to vary depending on dopant type and level, and conductivity behavior remains complex. While conductivity is of interest and the reason for further investigation into the rhombohedral phase, the central focus of this work is on structural stability and phase evolution rather than electrical performance.

By tailoring the dopant composition, any one of the rhombohedral, cubic, tetragonal or monoclinic phases (Fig. 1) can be formed. Jolley et al. [15] provided the first systematical study to explore the rhombohedral phase stability window in terms of the dopant content and average dopant cationic radius. They investigated sample compositions

* Corresponding author. 1 Jan Smuts Avenue, Johannesburg, South Africa.
E-mail address: caren.billing@wits.ac.za (C. Billing).

https://doi.org/10.1016/j.jssc.2025.125597
Received 14 June 2025; Received in revised form 6 August 2025; Accepted 18 August 2025
Available online 22 August 2025

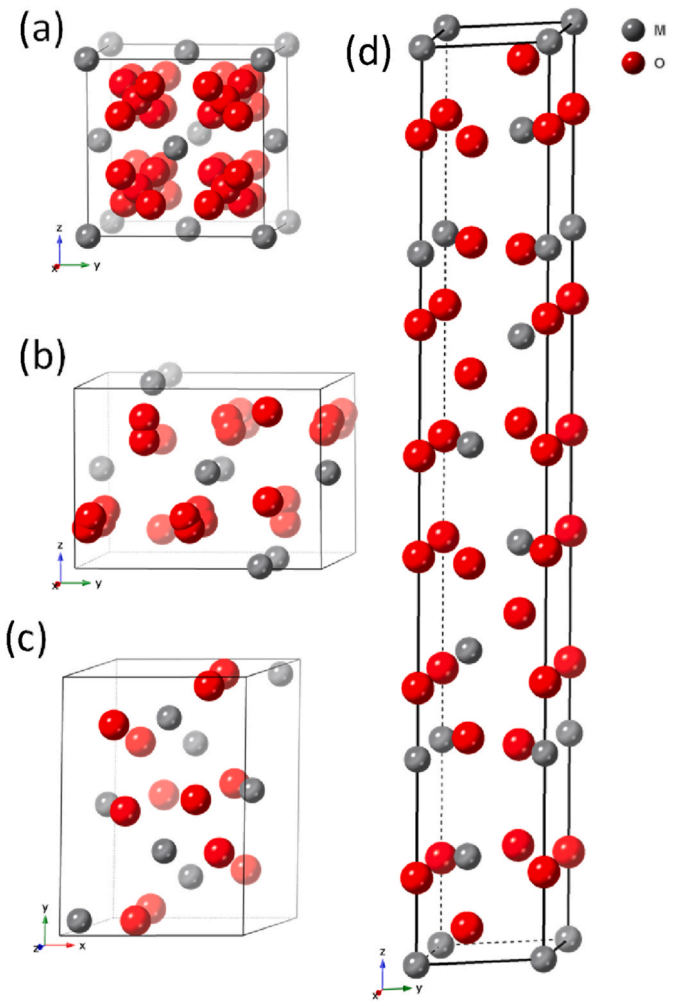

Fig. 1. Unit cells for the (a) face-centered cubic δ-phase (the 48i anionic site is omitted for clarity), (b) tetragonal β-phase, (c) monoclinic α-phase and (d) substituted rhombohedral phase of bismuth oxide. Grey and red spheres represent the cation and anion sites, respectively. The partial occupancy of all anionic sites has been omitted for clarity. (For interpretation of the references to colour in this figure legend, the reader is referred to the Web version of this article.)

comprising La^{3+}, Y^{3+}, Nd^{3+}, Ca^{2+}, and Sr^{2+} dopants with total dopant content between 6 and 10 %, representing a variation in the average cationic dopant radius between 1.06 and 1.15 Å. Mercurio et al. [20] roughly investigated the rhombohedral phase stability window over a significantly higher dopant content range, where several members of the Bi_2O_3-Ln_2O_3–TeO_2 (Ln = La, Sm or Gd) system were found to form the rhombohedral phase over a total dopant content range of 25–50 %, reflecting an average cationic dopant radius range of 1.012–1.097 Å. Takahashi et al. [16] investigated the Bi_2O_3–SrO system and found that the rhombohedral phase forms for 20–40 % SrO content (Sr^{2+} ionic radius = 1.260 Å). Additionally, Iwahara et al. [17] investigated the Bi_2O_3-Ln_2O_3 (Ln = La, Nd or Sm) system and found that the rhombohedral phase forms with 15–28 % La_2O_3, 10–30 % Nd_2O_3 and 30 % Sm_2O_3, reflecting a variation in the average cationic dopant radius range of 1.079–1.160 Å.

In this work, the rhombohedral phase stability windows already established [15–17,20], are further expanded by yttrium and lanthanum/aluminium co-doping. Our focus is on understanding how weighted average dopant cation radius and total dopant content influence phase formation, spanning broader ranges than previously reported. Furthermore, we investigate the high-temperature phase evolution and anisotropic thermal expansion behavior of selected rhombohedral-rich compositions using *in situ* synchrotron diffraction. These investigations provide new insights into the structural stability and thermal behavior of rhombohedral Bi_2O_3 systems, which are crucial considerations for their potential application as functional materials.

2. Materials and methods

2.1. Synthesis and sample preparation

All samples were prepared by means of a citrate sol-gel process [21]. Stoichiometric amounts of $Bi(NO_3)_3{\cdot}5H_2O$ (99.99 % pure, Sigma-Aldrich), $Y(NO_3)_3{\cdot}6H_2O$ (99.8 % pure, Sigma-Aldrich), $La(NO_3)_3{\cdot}6H_2O$ (99.99 % pure, Aldrich) and $Al(NO_3)_3{\cdot}9H_2O$ (99.99 % pure, Aldrich) were dissolved in acetic acid (98 % pure, MK Chemical) under moderate heating and stirring. Aqueous solutions were avoided to prevent the hydrolysis of Bi^{3+}. Excess citric acid (ACS reagent, Aldrich) was added, and the resulting mixture evaporated to form a metal complex paste. The dried gel was calcined at 450 °C for 18 h, then ground into a fine powder using an agate mortar and pestle and then annealed at 750 °C for 8 h to obtain the mixed metal oxide powders. Samples were prepared with varying substitution concentrations and are labelled to reflect this, for example, the 6 % Y_2O_3 + 9 % La_2O_3 substituted Bi_2O_3 sample is labelled as 6Y9LSB and the sample with 17 % Y_2O_3 + 3 % Al_2O_3 is labelled as 17Y3ASB.

2.2. Powder X-ray diffraction

Room temperature powder X-ray diffractograms were collected on a Bruker D2 Phaser using iron filtered CoK_α radiation (λ = 1.788 Å). *In situ* variable temperature powder diffractograms of selected samples were collected at beamline 28-ID-1 (λ = 0.1671 Å) at the National Synchrotron Light Source II (NSLS-II) [22]. Samples in quartz capillaries were heated using a hot air blower. The set temperature range of 450–850 °C was calibrated using the NIST standard reference material 640d (silicon powder) [23] and applying thermal lattice expansion corrections to the temperature profile [24,25], resulting in a corrected temperature range of 360–656 °C. Diffractograms were indexed using Bruker AXS DIFFRAC.EVA V4.2 and Rietveld refinement of the diffractograms was done using Bruker AXS TOPAS-Academic Version 6 [26]. In the refinements of the room temperature lab-based diffractograms, the instrument resolution function (IRF) [27] was determined using NIST 660a (LaB_6) and was described using the fundamental parameters approach [28] using the full axial divergence model [29] to account for divergence-related asymmetry of the diffraction peaks. In the refinements of the synchrotron *in situ* diffractograms, the IRF was determined using NIST 640d and was described using the Thompson Cox Hastings (TCHZ) Pseudo-Voigt function [30] with the divergence-related asymmetry effects described in an empirical way using the simple axial model [27]. In each refinement, the parameters refined were the scale factors, selected corrections, and lattice parameters. Atomic positional parameters were fixed to those published for the respective crystal structures and atomic thermal parameters were fixed to reasonable values.

2.3. Calculation of thermal expansion

The change in volume of rhombohedral Bi_2O_3 during heating is determined using equation (1):

$$\Delta V = \beta_v V_0 \Delta T \quad (1)$$

where ΔV is the change in unit cell volume, β_v is the volumetric coefficient of thermal expansion, V_0 is the initial unit cell volume and ΔT is the change in temperature. In this work, β_v is used to quantify the rate of thermal expansion of rhombohedral Bi_2O_3. Similarly, the thermal expansion behavior of cubic Bi_2O_3 during heating is determined using

equation (2):

$$\Delta L = \alpha_l L_0 \Delta T \quad (2)$$

where ΔL is the change in unit cell length, α_l is the linear coefficient of thermal expansion, L_0 is the initial unit cell length and ΔT is the change in temperature. For isotropic materials, $\beta_v = 3\alpha_l$ [31]. While rhombohedral Bi_2O_3 does exhibit some anisotropy, the approximation $\beta_v \approx 3\alpha_l$ (a derivation of this approximate relationship is given in the supplementary information) is used here to allow qualitative comparison with volumetric expansion data reported for isotropic cubic Bi_2O_3.

3. Results and discussion

3.1. Exploration of the rhombohedral phase stability window using powder X-ray diffraction

The region in which the phase stability window for the rhombohedral phase has been explored [15–17,20], in terms of the dopant content and particularly the weighted average dopant cationic radii, is significantly expanded utilizing a double doping methodology. The compositions were selected to span a wide range of average dopant cationic radii while maintaining isovalent substitution on the Bi^{3+} sublattice, allowing us to investigate how average dopant radius and chemical strain influence phase stability across a broad range. Lanthanum–yttrium and

Table 1
Substituted Bi_2O_3 compositions, weighted average cationic radius and quantitative phase content based on Rietveld refinement.

Name	Composition	Average dopant cationic radius (Å)	Phase content (weight %)		
			Cubic (*Fm* $\bar{3}$ m)	Tetragonal (*P* 4_2nmc)	Rhombohedral (*R* $\bar{3}$ m)
7.5 % dopant concentration					
6.5Y1ASB	$Bi_{0.925}Y_{0.065}Al_{0.01}O_{1.5}$	0.954	0	100	0
7.2Y0.3ASB	$Bi_{0.925}Y_{0.072}Al_{0.003}O_{1.5}$	1.000	0	100	0
5.5Y2LSB	$Bi_{0.925}Y_{0.055}La_{0.02}O_{1.5}$	1.057	30.6	69.4	0
3.4Y4.1LSB	$Bi_{0.925}Y_{0.034}La_{0.041}O_{1.5}$	1.096	3.0	2.2	94.8
2Y5.5LSB	$Bi_{0.925}Y_{0.02}La_{0.055}O_{1.5}$	1.122	1.6	4.3	94.1
10 % dopant concentration					
8.5Y1.5ASB	$Bi_{0.9}Y_{0.085}Al_{0.015}O_{1.5}$	0.946	26.7	73.3	0
9.5Y0.5ASB	$Bi_{0.9}Y_{0.095}Al_{0.005}O_{1.5}$	0.995	18.8	81.2	0
8.1Y1.9LSB	$Bi_{0.9}Y_{0.081}La_{0.019}O_{1.5}$	1.046	14.7	85.3	0
4Y6LSB	$Bi_{0.9}Y_{0.04}La_{0.06}O_{1.5}$	1.104	3.7	2.5	93.8
2.5Y7.5LSB	$Bi_{0.9}Y_{0.025}La_{0.075}O_{1.5}$	1.125	3.3	8.9	87.8
11-13 % dopant concentration					
10Y3ASB	$Bi_{0.87}Y_{0.1}Al_{0.03}O_{1.5}$	0.907	28.7	71.3	0
10Y2ASB	$Bi_{0.88}Y_{0.1}Al_{0.02}O_{1.5}$	0.938	35.4	64.6	0
10Y1ASB	$Bi_{0.89}Y_{0.1}Al_{0.01}O_{1.5}$	0.975	50.9	49.1	0
10Y1LSB	$Bi_{0.89}Y_{0.1}La_{0.01}O_{1.5}$	1.032	81.8	10.8	7.4
10Y2LSB	$Bi_{0.88}Y_{0.1}La_{0.02}O_{1.5}$	1.043	42.6	0	57.4
10Y3LSB	$Bi_{0.87}Y_{0.1}La_{0.03}O_{1.5}$	1.052	16.3	0	83.7
15 % dopant concentration					
13Y2ASB	$Bi_{0.85}Y_{0.13}Al_{0.02}O_{1.5}$	0.955	73.2	26.8	0
15YSB	$Bi_{0.85}Y_{0.15}O_{1.5}$	1.019	69.6	31.4	0
6Y9LSB	$Bi_{0.85}Y_{0.06}La_{0.09}O_{1.5}$	1.104	6.4	2.8	90.8
1Y14LSB	$Bi_{0.85}Y_{0.01}La_{0.14}O_{1.5}$	1.151	0	2.4	97.6
17.5 % dopant concentration					
15Y2.5ASB	$Bi_{0.825}Y_{0.15}Al_{0.025}O_{1.5}$	0.950	84.4	15.6	0
17.5YSB	$Bi_{0.825}Y_{0.175}O_{1.5}$	1.019	86.7	13.3	0
13.5Y4LSB	$Bi_{0.825}Y_{0.135}La_{0.04}O_{1.5}$	1.051	7.7	1.0	91.3
7.5Y10LSB	$Bi_{0.825}Y_{0.075}La_{0.1}O_{1.5}$	1.100	3.9	3.2	92.9
1.5Y16LSB	$Bi_{0.825}Y_{0.015}La_{0.16}O_{1.5}$	1.148	0	0	100
20 % dopant concentration					
17Y3ASB	$Bi_{0.8}Y_{0.17}Al_{0.03}O_{1.5}$	0.946	94.6	5.4	0
19Y1ASB	$Bi_{0.8}Y_{0.19}Al_{0.01}O_{1.5}$	0.995	97.3	2.7	0
16Y4LSB	$Bi_{0.8}Y_{0.16}La_{0.04}O_{1.5}$	1.047	8.2	2.0	89.8
8Y12LSB	$Bi_{0.8}Y_{0.08}La_{0.12}O_{1.5}$	1.104	0	4.5	95.5
1Y19LSB	$Bi_{0.8}Y_{0.01}La_{0.19}O_{1.5}$	1.153	0	0	100
22.5 % dopant concentration					
19.5Y3ASB	$Bi_{0.775}Y_{0.195}Al_{0.03}O_{1.5}$	0.954	90.4	9.6	0
21.5Y1ASB	$Bi_{0.775}Y_{0.215}Al_{0.01}O_{1.5}$	0.997	92.1	7.9	0
17.5Y5LSB	$Bi_{0.775}Y_{0.175}La_{0.05}O_{1.5}$	1.050	9.7	0	90.3
10Y12.5LSB	$Bi_{0.775}Y_{0.1}La_{0.125}O_{1.5}$	1.097	3.5	0	96.5
1.5Y21LSB	$Bi_{0.775}Y_{0.015}La_{0.21}O_{1.5}$	1.151	0	0	100
25 % dopant concentration					
20Y5ASB	$Bi_{0.75}Y_{0.2}Al_{0.05}O_{1.5}$	0.922	100	0	0
21Y4ASB	$Bi_{0.75}Y_{0.21}Al_{0.04}O_{1.5}$	0.942	100	0	0
22Y3ASB	$Bi_{0.75}Y_{0.22}Al_{0.03}O_{1.5}$	0.961	100	0	0
23Y2ASB	$Bi_{0.75}Y_{0.23}Al_{0.02}O_{1.5}$	0.980	100	0	0
24Y1ASB	$Bi_{0.75}Y_{0.24}Al_{0.01}O_{1.5}$	1.000	100	0	0
24Y1LSB	$Bi_{0.75}Y_{0.24}La_{0.01}O_{1.5}$	1.025	100	0	0
23Y2LSB	$Bi_{0.75}Y_{0.23}La_{0.02}O_{1.5}$	1.030	89.5	0	10.5
22Y3LSB	$Bi_{0.75}Y_{0.22}La_{0.03}O_{1.5}$	1.036	63.0	0	37.0
21Y4LSB	$Bi_{0.75}Y_{0.21}La_{0.04}O_{1.5}$	1.042	21.2	0	78.8
20Y5LSB	$Bi_{0.75}Y_{0.2}La_{0.05}O_{1.5}$	1.047	18.0	0	82.0
10Y15LSB	$Bi_{0.75}Y_{0.1}La_{0.15}O_{1.5}$	1.104	0	0	100
1Y24LSB	$Bi_{0.75}Y_{0.01}La_{0.24}O_{1.5}$	1.154	0	0	100

aluminum–yttrium co-doped systems were investigated where, by systematic variation of the Y:La and Y:Al ratios, fine control over average cation radius is enabled. La^{3+} (1.16 Å, CN = 8 where CN is the coordination number) closely matches the ionic radius of Bi^{3+} (1.17 Å, CN = 8) [32], resulting in minimal lattice strain and promoting rhombohedral phase stabilization. In contrast, Y^{3+} (1.019 Å, CN = 8) and especially Al^{3+} (0.535 Å, CN = 6) [32] are significantly smaller, introducing increased levels of lattice strain. Notably, Al^{3+} strongly favors octahedral coordination, which may not be easily accommodated in the 8-fold coordination typical of Bi^{3+} sites, potentially leading to local structural strain which is more readily accommodated in other phases. This design allows systematic investigation of how dopant size and structural strain influence polymorphic phase stability, transformation pathways, and the persistence of metastable phases under thermal treatment.

Using a dopant concentration range of 7.5–25 %, the weighted average dopant radius of 0.907–1.154 Å was probed. Table 1 summarizes the substituted Bi_2O_3 compositions investigated, and the associated phase content as determined from Rietveld analysis of the X-ray diffractograms (Figs. 2 and 3). Calculated diffractograms of the cubic, tetragonal and rhombohedral phases are included for easy visual assessment of the phases present.

At a total dopant concentration of 7.5 %, the relative dopant cationic radius was varied between 0.954 and 1.122 Å by altering the ratio of Y to La and Y to Al (Fig. 2a and Table 1). At this dopant level, Jolley et al. [15] predicted a pure rhombohedral phase to be present over an average dopant radius range of ~1.10-1.14 Å, but in this work a pure

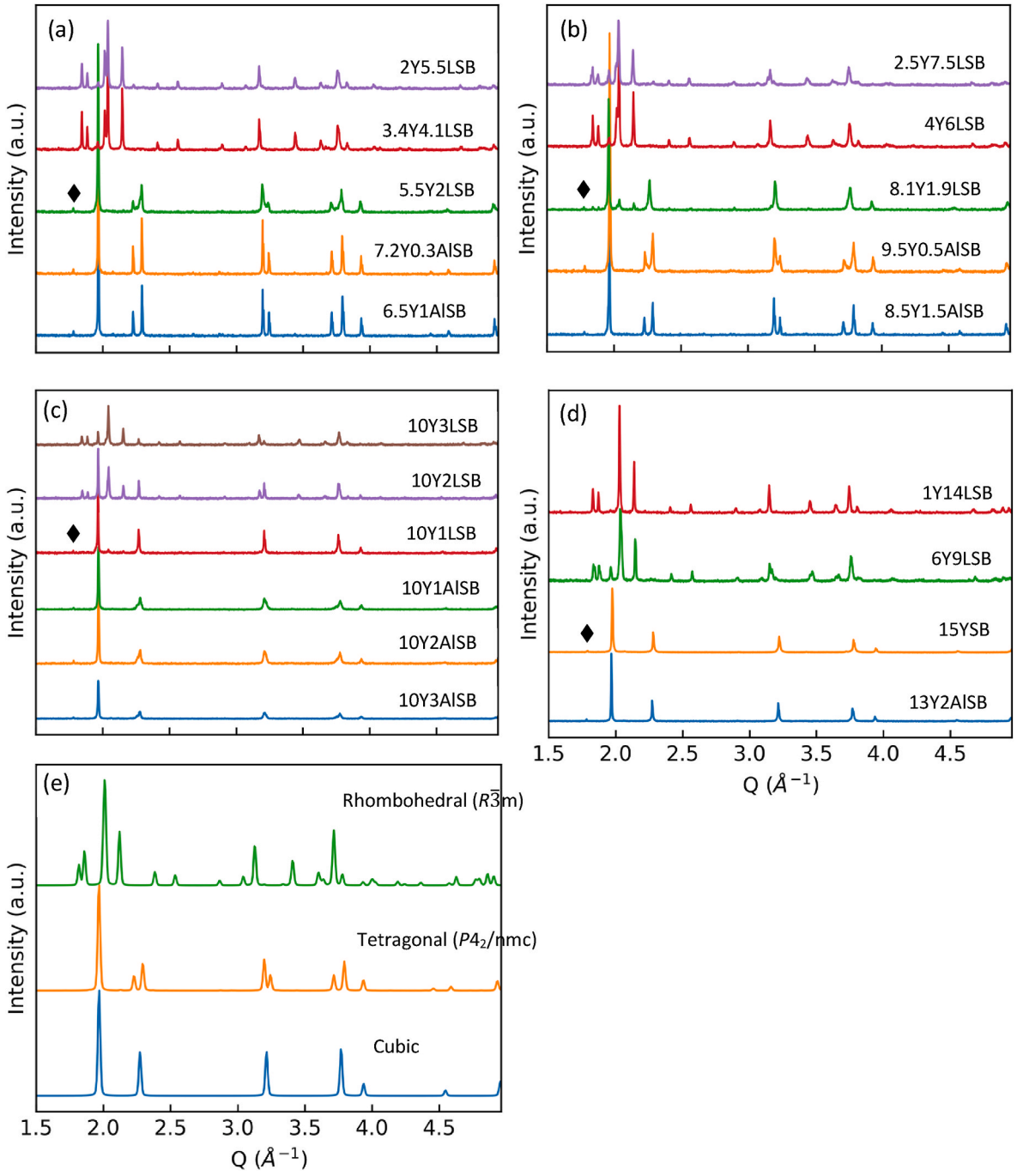

Fig. 2. Room temperature diffractograms of doped bismuthates with (a) 7.5 %, (b) 10 %, (c) 11–13 % and (d) 15 % total dopant content. K_β reflections are shown with ◆ symbols. (e) Calculated diffractograms of the cubic, tetragonal and rhombohedral phases.

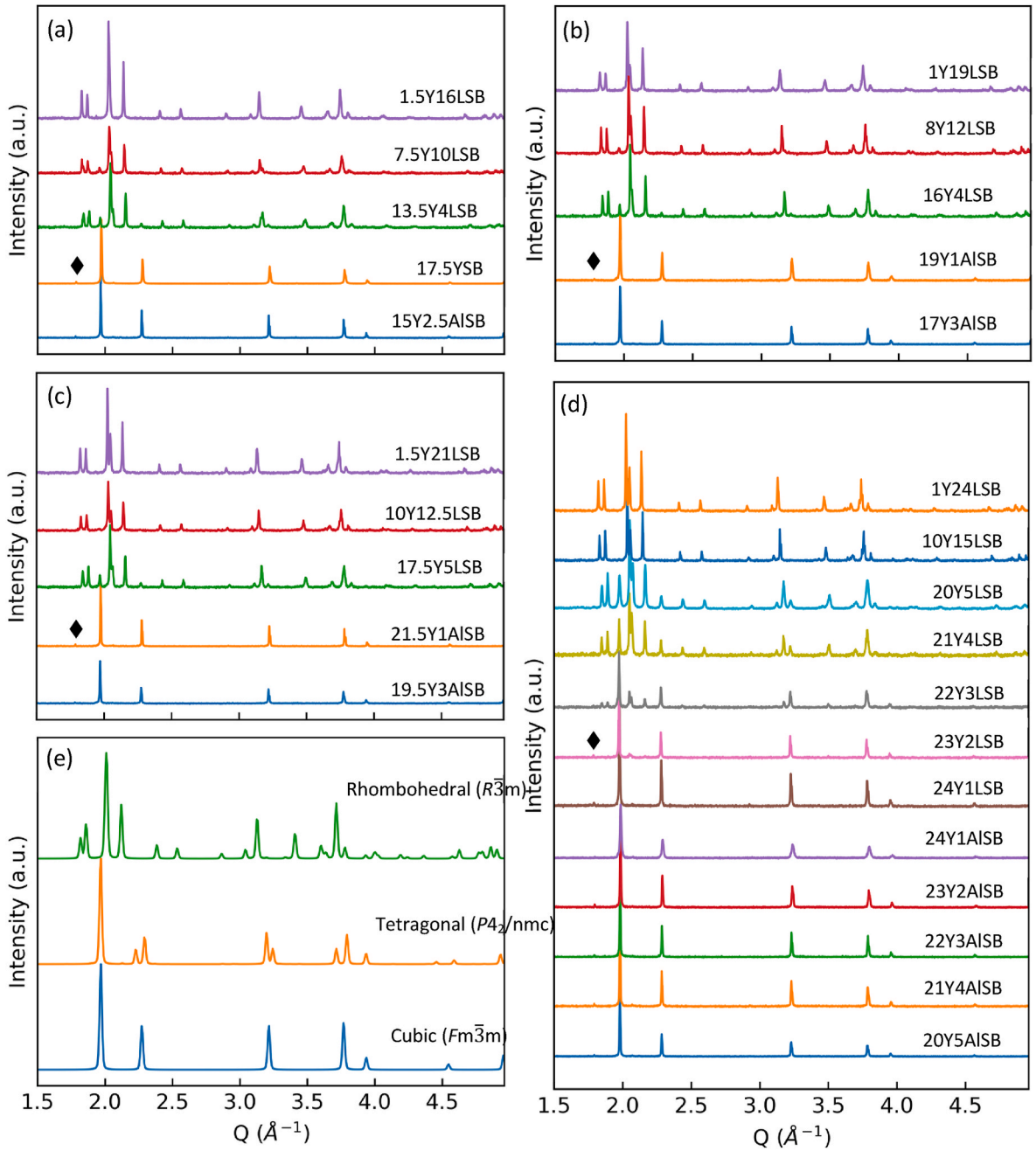

Fig. 3. Room temperature diffractograms of doped bismuthates with (a) 17.5 %, (b) 20 %, (c) 22.5 % and (d) 25 % total dopant content. K_β reflections are shown with ◆ symbols. (e) Calculated diffractograms of the cubic, tetragonal and rhombohedral phases.

rhombohedral phase was not formed. Over the average dopant radius range of 0.954–1.000 Å, using Y and Al dopants, a pure tetragonal phase was present. The Rietveld analysis of the 7.2Y0.3ASB sample is given in Fig. 4a as an example. At an average dopant radius of 1.057 Å, using Y and La as dopants, a cubic and tetragonal phase mixture was present and over the range of 1.096–1.122 Å, rhombohedral-rich phase mixtures, comprising both cubic and tetragonal phases in minor quantities, were evident. The Rietveld analysis of the 2Y5.5LSB sample is given in Fig. 4b as an example of the rhombohedral-rich phase mixture.

The rhombohedral phase window was similarly investigated at a significantly higher dopant concentration of 25 % (Table 1). Over an average dopant radius range of 0.922–1.025 Å the pure cubic phase was present, and the Rietveld analysis of the 20Y5ASB sample is illustrated in Fig. 5a. Between 1.030 and 1.047 Å, for samples doped with Y and La, cubic and rhombohedral phase mixtures were present, and rhombohedral phase content increased with increasing average cationic dopant radius. The Rietveld analysis of the 22Y3LSB sample is shown in Fig. 5b. Between 1.104 and 1.154 Å, for samples also doped with Y and La, pure rhombohedral phase was present and the Rietveld analysis of the 1Y24LSB sample is given in Fig. 5c. The rhombohedral phase presence over this range somewhat coincides with the rhombohedral phase stability window established by Iwahara et al. [17].

In the region between these two extremes, the rhombohedral phase window was further investigated from 10 to 22.5 % total dopant concentration over an average dopant cationic radius range of 0.909–1.153 Å (Table 1). Over this wide range, phase mixtures were almost entirely present. Pure rhombohedral phase was only present at an average dopant radius of approximately 1.15 Å (the maximum radius investigated in this work) in the 17.5–22.5 % total dopant range. Notably, at 10 % total dopant concentration Jolley et al. [15] predicted pure

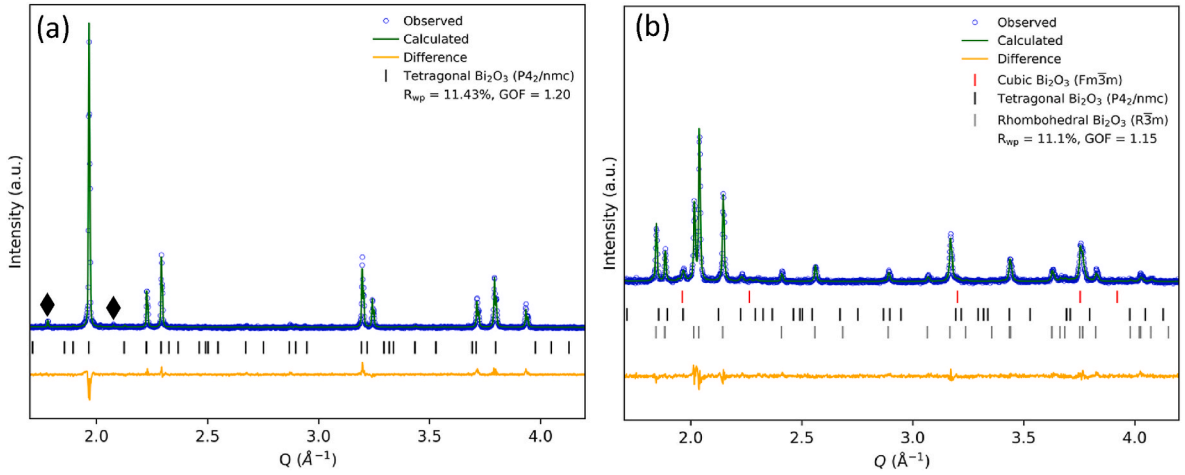

Fig. 4. Room temperature diffractograms showing Rietveld refinement analysis for the (a) 7.2Y0.3ASB and (b) 2Y5.5LSB materials, both having a 7.5 % total dopant concentration. The observed pattern is shown in blue, the calculated in green and the difference in orange. Miller indices corresponding to the cubic, tetragonal, and rhombohedral phases are shown with red, black and grey ticks, respectively. K_β reflections are shown with ◆ symbols. (For interpretation of the references to colour in this figure legend, the reader is referred to the Web version of this article.)

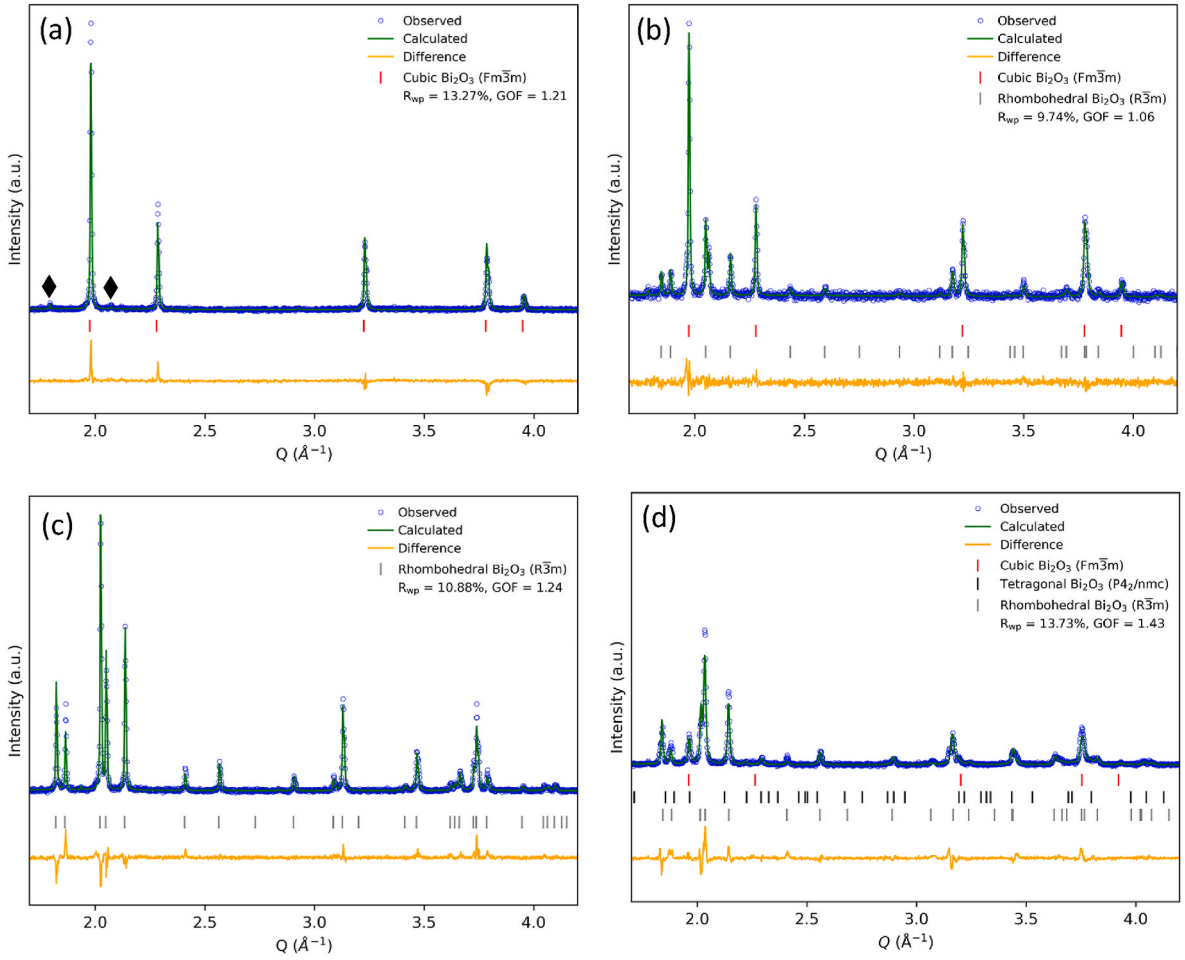

Fig. 5. Room temperature diffractogram showing Rietveld refinement analysis for the (a) 20Y5ASB, (b) 22Y3LSB, (c) 1Y24LSB and (d) 2.5Y7.5LSB materials. The observed pattern is shown in blue, the calculated in green and the difference in orange. Miller indices corresponding to the cubic, tetragonal, and rhombohedral phases are shown with red, black and grey ticks, respectively. K_β reflections are shown with ◆ symbols. (For interpretation of the references to colour in this figure legend, the reader is referred to the Web version of this article.)

rhombohedral doped Bi_2O_3 to be present over an average dopant cationic radius range of ~1.065-1.14 Å, using Y and La as dopants. In this work over the same range, phase mixtures were evident with the rhombohedral phase being dominant. The Rietveld analysis of the 2.5Y7.5LSB sample clearly shows the presence of a cubic-tetragonal-rhombohedral phase mixture at 10 % total dopant content and an average dopant cationic radius of 1.125 Å in Fig. 5d. The stabilization of different Bi_2O_3 polymorphs is governed by the average cationic radius, total dopant level and preferred dopant coordination number. Small, rigid cations like Al^{3+}, which favor low coordination numbers (4–6) [32], tend to introduce local lattice contraction and reduce structural flexibility, thereby promoting stabilization of the high-symmetry cubic phase. In contrast, larger dopants such as La^{3+} or Y^{3+} which favor higher coordination numbers (7–9) [32], are more compatible with the coordination environment of Bi^{3+}. This compatibility permits local distortions and anisotropic bonding, enabling the stabilization of lower-symmetry rhombohedral or tetragonal phases. Thus, the dopant's ability to accommodate distorted coordination geometries, reflected in both ionic size and coordination number, plays a central role in determining the sequence and stability of phase transitions in doped Bi_2O_3 systems. We see a clear example of this at 25 % total dopant concentration where high Al^{3+} content results in exclusive formation of the cubic phase across an average dopant ionic radius of 0.922–1.000 Å. At the same dopant level, La^{3+} content strongly favors formation of the lower symmetry rhombohedral phase (Table 1). Similarly, at 11–13 % total dopant concentration, over an average dopant cationic radius of 0.907–1.052 Å, we observe increasing Al^{3+} content to promote the formation the tetragonal phase while increase La^{3+} content favors the lower symmetry rhombohedral formation.

The rhombohedral phase stability window established in this work only somewhat coincides with that established by Iwahara et al. [17] (Fig. 6). Takahashi et al. [16] used Sr as a dopant which resulted in a significantly higher average dopant cationic radius region than considered here. Mercurio et al. [20] also studied significantly higher total dopant concentrations in comparison to that investigated in this work, however, they did report pure rhombohedral phase at 25 % dopant concentration and average dopant radius of ~1.05 Å using La and Te as dopants. In this work, for the same dopant level and average dopant cationic radius, only 82 % rhombohedral phase was present when using La and Y as dopants (Fig. 6 and Table 1). As mentioned, the rhombohedral phase stability window established by Jolley et al. [15] did not match the findings in a similar region in this work despite La and Y dopants being used in both cases. These discrepancies are likely due to the varying synthetic methodologies utilized. In this work, a soft chemical citrate gel technique was used to synthesize material precursors which were calcined at 450 °C and then annealed at 750 °C in air to yield the final material. Jolley et al. [15] employed a standard solid state synthesis route with both calcination and subsequent sintering done at 800 °C in air. Takahashi et al. [16] also employed a solid state synthesis technique, calcining at 700–800 °C and subsequently sintering between 800 and 1000 °C in air (compositionally dependent sintering temperature). Similarly, Iwahara et al. [17] used a solid state synthesis technique, with calcination at 800–1100 °C and subsequent sintering between 850 and 1150 °C in air (compositionally dependent sintering temperature). Although Mercurio et al. [20] also did solid state synthesis, there were a few key differences. The individual metal oxides were initially annealed at 800–900 °C for 24 h in a pure nitrogen atmosphere. Thereafter, powder samples were annealed for 24 h at 800 °C and then either air quenched or allowed to slowly cool to room temperature. These variations in the synthetic methodology are likely responsible, at least in part, for the observed differences in the phase stability window of the rhombohedral phase.

3.2. *In situ phase transformation behavior of 2Y5.5LSB and 2.5Y7.5LSB*

Rhombohedral doped Bi_2O_3 materials have demonstrated promising ionic conductivity at temperatures suitable for intermediate-to-low temperature SOFCs electrolytes [15,17,20]. For such applications, high structural stability during thermal cycling is essential, as well as exhibiting a low, and ideally linear, rate of thermal expansion. Two materials, 2Y5.5LSB and 2.5Y7.5LSB, were investigated in this work over the temperature range of 360–656 °C. These compositions have the lowest total dopant content within the studied range, which is typically considered favorable for maximizing ionic conductivity [15], but they merely produce rhombohedral-rich phase mixtures (94 % and 88 % rhombohedral for 2Y5.5LSB and 2.5Y7.5LSB, respectively) at room temperature (Table 1, Fig. 4b and 5d). The thermal behavior of these heterogeneous samples was investigated both to evaluate the stability of

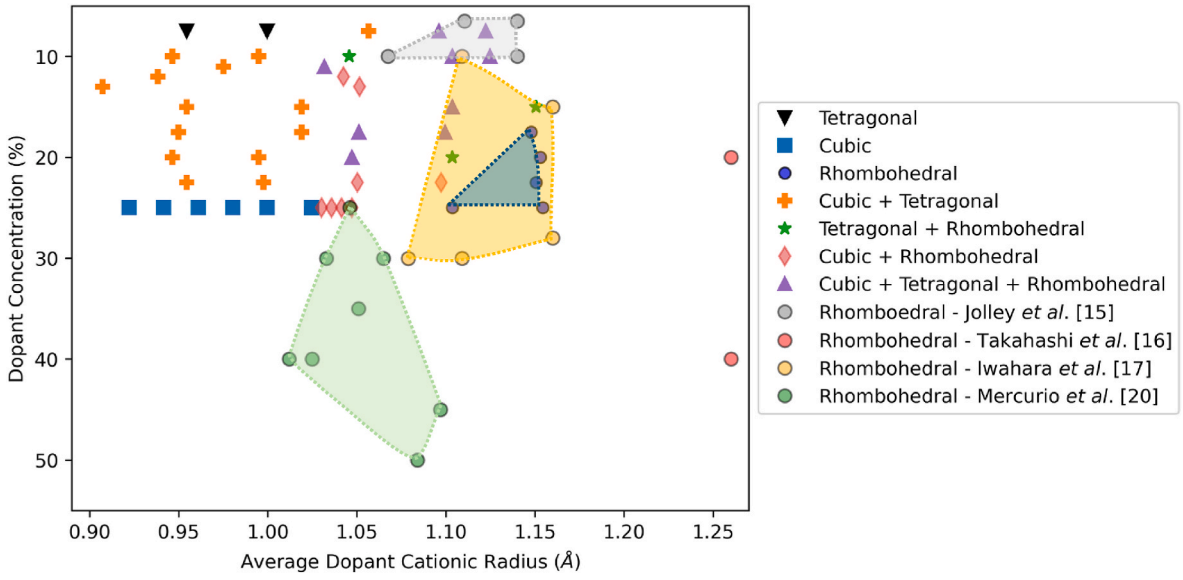

Fig. 6. Approximate phase stability window of rhombohedral Bi_2O_3 identified in this work (blue area), by Jolley et al. [15] (grey region), Iwahara et al. [17] (yellow region) and by Mercurio et al. [19] (green region) given as a function of total dopant content and average dopant cationic radius. Phase compositions identified at various dopant concentrations and average dopant cationic radii are indicated. (For interpretation of the references to colour in this figure legend, the reader is referred to the Web version of this article.)

the rhombohedral phase and to understand how coexisting minor phases evolve, interact, or transform upon heating. This approach offers insights into the thermal robustness of rhombohedral-rich materials, where phase purity could be compromised due to thermal cycling or where impurity phases are below the detection limit, especially when laboratory-based X-ray diffractometers are used.

Upon heating from room temperature to 360 °C, the 2Y5.5LSB material (with initial phase composition of 94.1 % rhombohedral, 4.3 % tetragonal and 1.6 % cubic (Table 1)), exhibited unchanged rhombohedral phase content while 5.9 % tetragonal phase content was observed

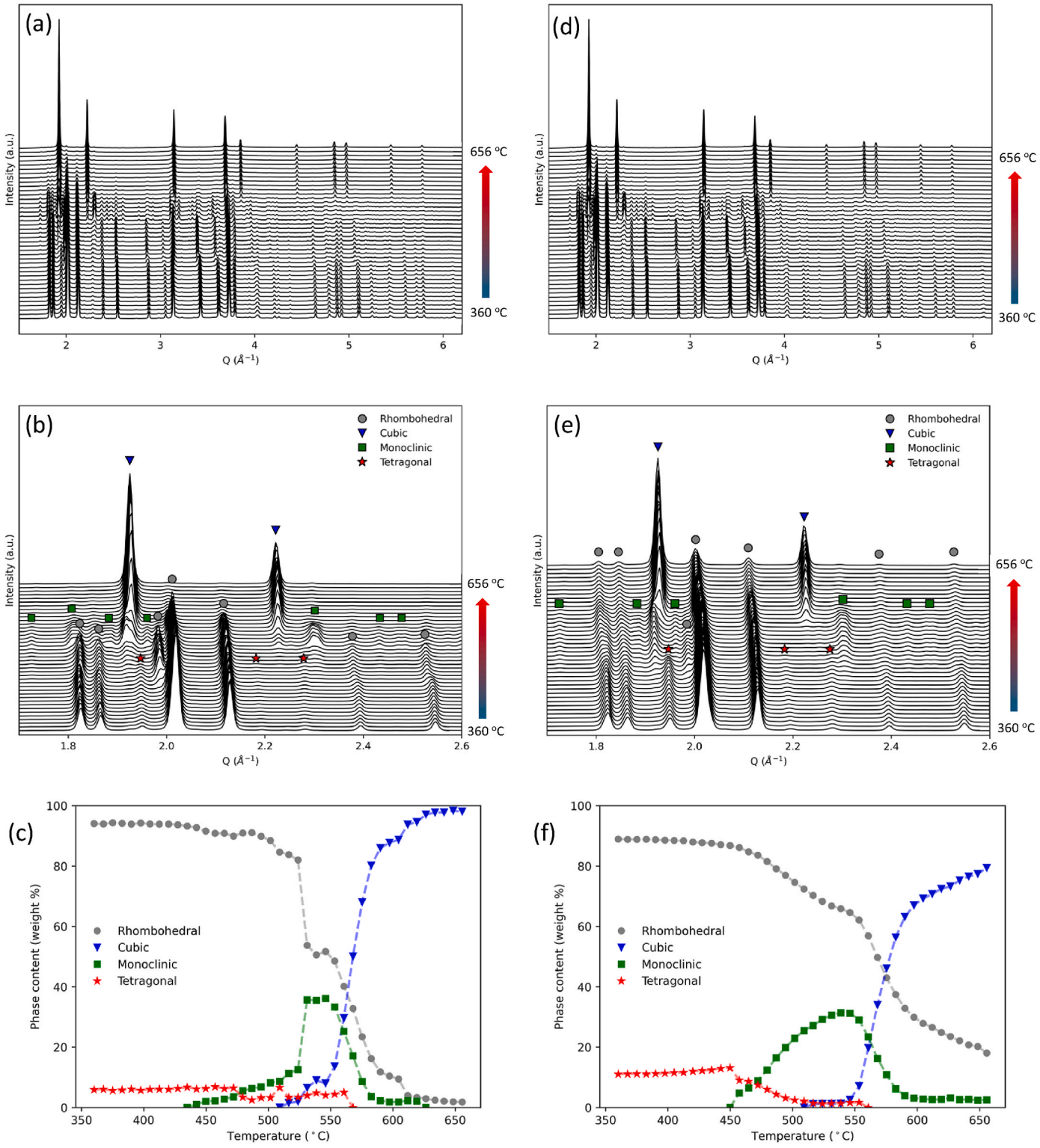

Fig. 7. (a) Diffractograms of the 2Y5.5LSB sample collected at ~7 °C intervals over the temperature range of 360–656 °C with (b) complex phase transitions indicated over the *Q* range of 1.7–2.6 Å^{-1} and (c) phase content variation over 360–656 °C. (d) Diffractograms of the 2.5Y7.5LSB sample collected at ~7 °C intervals over the temperature range of 360–656 °C with (e) complex phase transitions indicated over the *Q* range of 1.7–2.6 Å^{-1} and (f) phase content variation over 360–656 °C.

(Fig. 7a–c). If trace cubic phase content remained, it was below the detection limits of the measurements. On further heating, the rhombohedral-tetragonal phase mixture was maintained until ~440 °C when a monoclinic phase ($P2_1/c$, SG #14 with unit cell volume ≈ 339 Å^3), ICSD: 15072) additionally formed, coinciding with a slight decrease in rhombohedral phase content indicative of a rhombohedral-to-monoclinic phase transformation. The monoclinic phase content increased sharply from ~525 °C and peaked at ~540 °C, which coincided with a sharp decrease in rhombohedral phase content and a minor increase in cubic phase content. The Rietveld analysis at ~545 °C, showing the individual phase contributions to the overall fit, is presented in Fig. 8. Above ~550 °C the monoclinic phase content decreased sharply and was no longer present by ~625 °C. From ~550 °C, there was a sharp decrease in the rhombohedral phase content and a corresponding sharp increase in cubic phase content representing the rhombohedral-to-cubic phase transition. Similarly, Jolley et al. [19] reported that $Bi_{0.9}La_{0.051}Y_{0.014}O_{1.5}$ undergoes a rhombohedral-to-cubic phase transition at temperatures above 580 °C. Additionally, above ~550 °C the tetragonal phase was no longer detected and by 656 °C the material was predominantly cubic with trace rhombohedral phase content of ~1.8 %.

For the 2.5Y7.5LSB material at 360 °C, 88.9 % rhombohedral and 11.1 % tetragonal phase content was present (Fig. 7d–f) compared to 87.8 % rhombohedral, 8.9 % tetragonal and 3.3 % cubic phase content at room temperature (Table 1), likely indicating cubic-to-tetragonal phase conversion. On further heating (Fig. 7e and f), the rhombohedral-tetragonal phase mixture was maintained until ~450 °C with a slight increase in tetragonal phase content and corresponding decrease in rhombohedral phase content. From ~450 °C gradual monoclinic phase formation was observed, reaching a maximum at ~550 °C. This formation coincided with a decrease in tetragonal and rhombohedral phase content, with the tetragonal phase disappearing by ~560 °C. For both compositions, it appears that a direct rhombohedral to monoclinic phase transformation occurred during heating, a phenomenon that has not been reported before. Above ~550 °C, the monoclinic phase content decreased sharply and plateaued at trace quantity level until ~656 °C. The onset of the rhombohedral-to-cubic phase transition was observed at ~550 °C. For 2.5Y7.5LSB (with a total dopant concentration of 10 %), a mixture of cubic, rhombohedral, and monoclinic phases was detected at ~656 °C (Fig. 7f), in contrast to the phase transition behavior of 2Y5.5LSB (with 7.5 % total dopant concentration) shown in Fig. 7c.

While the overall phase change behavior is similar across both compositions, subtle differences exist which stem from a combined effect of both total dopant concentration and average dopant cationic radius. The higher total dopant content of 2.5Y5.5LSB is expected to enhance the overall phase stability of the system. Additionally, the larger average cationic radius of 2.5Y7.5LSB is also expected to introduce greater lattice strain. Together, these features likely favor (thermodynamically and kinetically) the persistence of the lower-symmetry rhombohedral and monoclinic phases. This contrasts with 2Y5.5LSB, which undergoes a cleaner and more complete transition to the cubic phase by 656 °C due to its lower dopant level and reduced internal strain.

3.3. Thermal expansion behavior of 2Y5.5LSB and 2.5Y7.5LSB

The thermal expansion behavior of specifically the rhombohedral phase of 2Y5.5LSB and 2.5Y7.5LSB was monitored from 360 to 656 °C (Figs. 9 and 10, respectively). Based on the rhombohedral crystal structure, this was done by monitoring changes in the unit cell volume, as well as in the *a* and *c* directions of the unit cell. Changes in these cell parameters were found to correlate with various phase changes for both materials. Similar behavior has been observed by Thrall et al. [33] for $BiFeO_3$, Struzik et al. [34] for $Bi_{14}YO_{22.5}$ and Borowska-Centkowska et al. [35] for $Bi_{14}WO_{24}$.

For 2Y5.5LSB, the volumetric expansion (Fig. 9a) and expansion in both the *a* and *c* directions (Fig. 9b) is linear between 360 and 450 °C. At ~450 °C, there is an abrupt increase in rhombohedral unit cell volume, along with abrupt expansion and contraction in the *c* and *a* directions, respectively. The expansion in the *c* direction dominates and results in the overall increase in unit cell volume. This anisotropic distortion

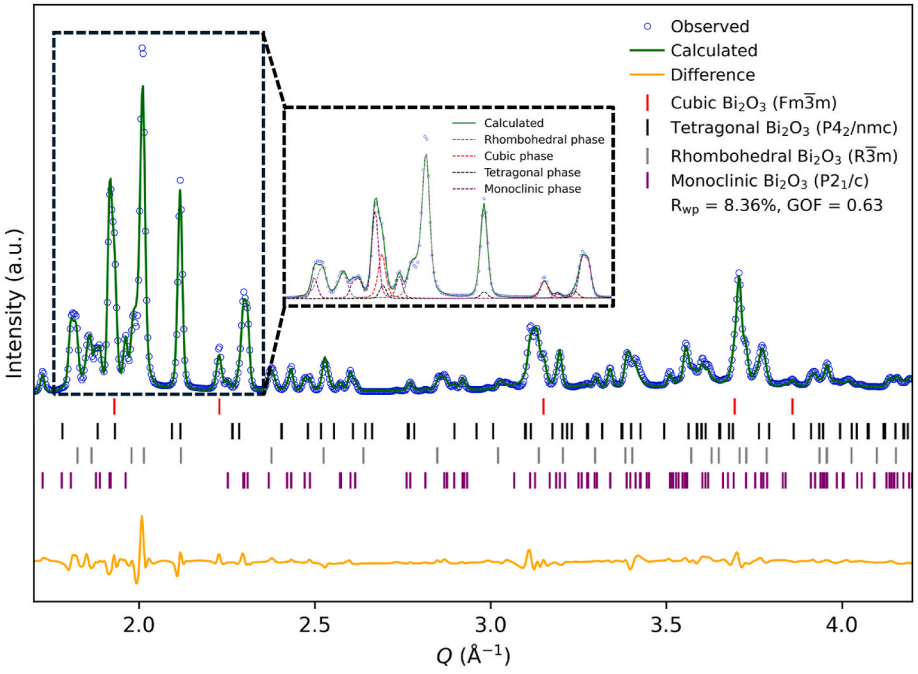

Fig. 8. Diffractogram showing Rietveld refinement analysis for 2Y5.5LSB at ~545 °C. The observed pattern is shown in blue, the calculated in green and the difference in orange. Miller indices corresponding to the cubic, tetragonal, rhombohedral and monoclinic phases are shown with red, black, grey and purple ticks, respectively. Individual phase contributions to the overall fit are shown in the inset. (For interpretation of the references to colour in this figure legend, the reader is referred to the Web version of this article.)

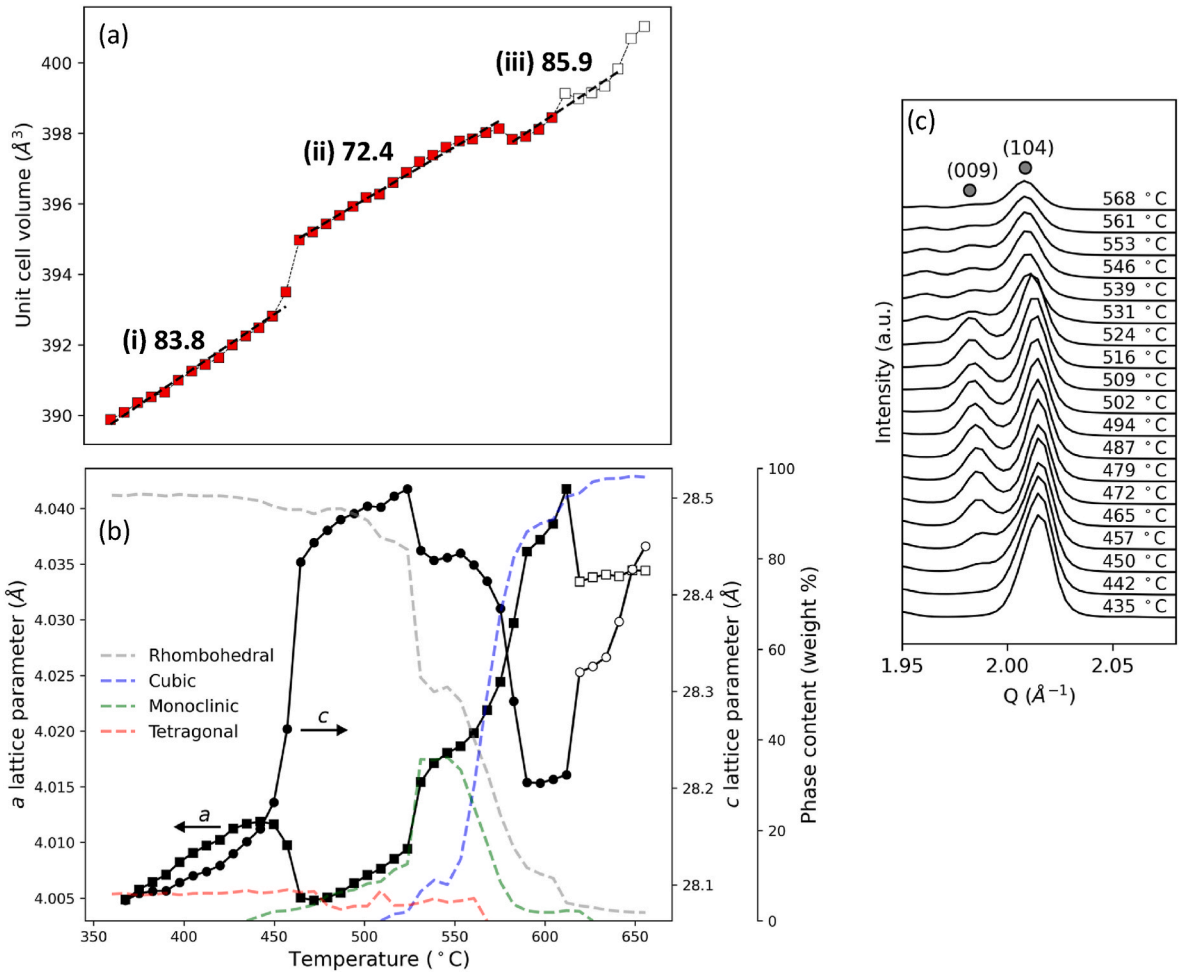

Fig. 9. Variation in (a) unit cell volume and (b) a (■ symbols) and c (● symbols) lattice parameters for the rhombohedral phase of 2Y5.5LSB over 360–656 °C. β_y for each linear region are given in (a). Open markers in (a) and (b) indicate the region of low rhombohedral phase content (<5 %) and in (b) the variation in phase composition shown in Fig. 7c is reproduced. (c) Separation of the (009) and (104) reflections of the rhombohedral phase are shown from 435 to 568 °C.

coincides with the formation of the monoclinic phase from ~450 °C suggesting that structural instability at this transition point promotes the formation of a lower symmetry phase. Additionally, a distinct separation of the (009) and (104) reflections for the rhombohedral phase (Fig. 9c) is observed. This peak separation was previously reported by Payzant et al. [36] for rhombohedral $Bi_{1.6}Sr_{0.2}O_{2.6}$ and attributed to a β_2-to-β_1 rhombohedral phase transition. This transition does not alter the symmetry of the structure but involves an abrupt expansion in the c axis direction due to the relaxation of bonds parallel to the c axis. High temperature neutron diffraction experiments by Mercurio et al. [37] reported that this phenomenon is due to the migration of oxygen ions into planes normal to the c axis. Payzant and King [38] later showed that for rhombohedral $(Bi_2O_3)_{1-x}(SrO)_x$ (x = 0.18–0.40) there is also an abrupt increase in the a parameter corresponding to the β_2-to-β_1 phase transition, although this discontinuity is far less prominent in comparison to that in the c direction. Mercurio et al. [37] and Conflant et al. [39,40] also showed that the β_2-to-β_1 phase transition can be directly observed from peak shifts in variable temperature diffractograms, emanating from the abrupt increase in lattice dimensions. As such, the separation of the (009) and (104) reflections and increase in the c parameter noted can be attributed to the β_2-to-β_1 phase transition starting at ~450 °C, although the simultaneous contraction of the a parameter was not previously observed (Fig. 9b). This could be an effect of the lower symmetry monoclinic phase formation which coincides with the β_2-to-β_1 phase transition. Additionally, the onset of the β_2-to-β_1 phase transition for 2Y5.5LSB is observed at a much lower temperature (~450 °C) compared to ~650 °C for $Bi_{0.75}Sr_{0.25}O_{1.375}$ [37], ~600–710 °C for $(Bi_2O_3)_{1-x}(SrO)_x$ (x = 0.18–0.42) [38], ~735–740 °C for $Bi_{1.5}Ca_{0.25}O_{2.5}$ [39] and ~530–610 °C for $Bi_{0.844}Ba_{0.156}O_{1.422}$ [40]. Payzant and King [38] also reported the dependance of the transition temperature on dopant concentration level for rhombohedral phase pure $(Bi_2O_3)_{1-x}(SrO)_x$ (x = 0.18–0.42) synthesized via conventional solid-state methods. The transition temperature decreased with decreasing dopant content below x = 0.28, however, they did not investigate compositions below x = 0.18. The low transition temperatures observed for 2Y5.5LSB with 7.5 % dopant content (and 2.5Y7.5LSB with 10 % dopant content as discussed below) thus agree with this general trend. These materials are also complicated by the fact that they contain two dopants and are mixed phase materials, factors which may contribute to the lower transition temperatures observed.

Between ~470 and 575 °C, another linear volumetric thermal expansion region is observed (Fig. 9a) despite there being another abrupt change in the individual lattice parameters at ~523 °C. This involves an expansion and simultaneous contraction in the a and c directions, respectively (Fig. 9b), which result in a negligible effect on the overall unit cell volume. These abrupt changes coincide with rapid growth of the monoclinic phase (to its maximum content), a sharp decrease in the rhombohedral phase and the onset of the cubic phase (Fig. 7c). The increase in monoclinic phase content likely enables the strain of the rhombohedral phase to be relieved, resulting in the c-direction contraction and a-direction expansion. Similarly, on further heating to ~575 °C another abrupt change in the expansion and

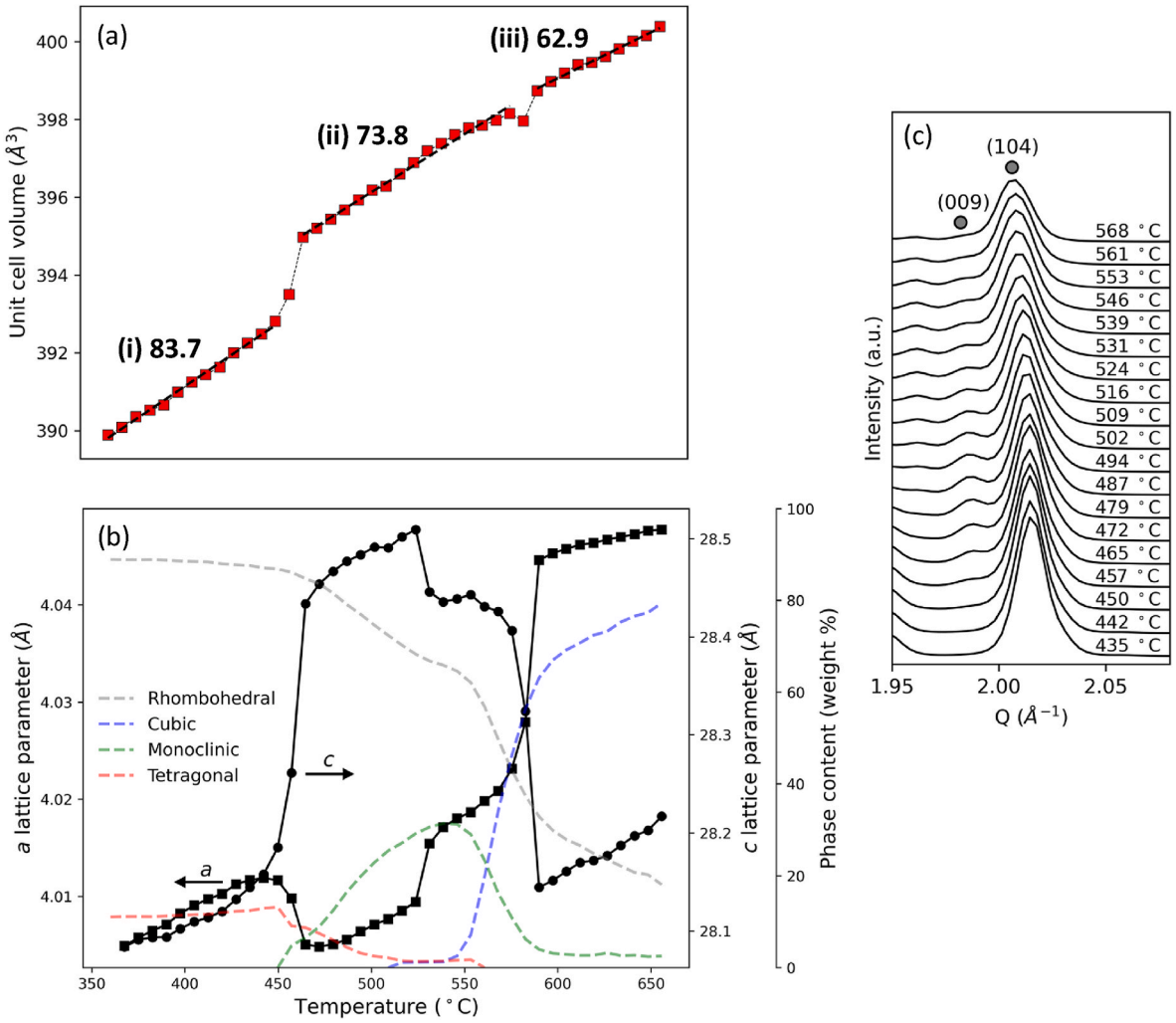

Fig. 10. Variation in (a) unit cell volume and (b) *a* (■ symbols) and *c* (● symbols) lattice parameters of the rhombohedral phase of 2.5Y7.5LSB over 360–656 °C. β_v for each linear region are given in (a). In (b) the variation in phase composition shown in Fig. 7f is reproduced. (c) Separation of the (009) and (104) reflections of the rhombohedral phase are shown over 435–568 °C. (a) Stabilization of rhombohedral Bi_2O_3 reflects an interplay between dopant nature and concentration, average dopant cationic radius and synthetic method. (b) Phase transformations of rhombohedral-rich mixture correlate with rhombohedral phase thermal expansion. Notably: rhombohedral β_2-to-β_1 transition at ~450 °C causes *a* contraction and *c* expansion and an intermediate monoclinic polymorph formation is observed from ~450 °C.

contraction rates in the *a* and *c* directions, respectively, is indicative of the rapid growth of the cubic phase and simultaneous reduction of the rhombohedral and monoclinic phases. Boivin and Thomas [41] reported the rhombohedral to cubic phase transformation of $Bi_{0.851}Sr_{0.149}O_{0.676}$ to occur at ~690 °C. This transformation occurred in a lower temperature range for 2Y5.5LSB (and 2.5Y7.5LSB as discussed below), again attributed to lower total dopant concentration and strain, the use of multiple dopants and the presence of multiple phases.

Further thermal expansion with abrupt changes in the *a* and *c* directions are observed on heating to ~611 °C, corresponding to the rapid disappearance and formation of the rhombohedral and cubic phases, respectively. Above ~611 °C, lattice parameters are less accurate due to the low rhombohedral phase content (<5 %, depicted with open markers in Fig. 8a and b). At 656 °C, the 2Y5.5LSB material comprised 98.2 % cubic and 1.8 % rhombohedral phase content.

It is thus seen that the anisotropic thermal expansion behavior of the rhombohedral phase is indicative not only of the β_2-to-β_1 phase transition, but also of the various other polymorphic phase transformations which occur during heating. This anisotropic thermal expansion points to a concerted system where the rhombohedral phase transforms to a lower symmetry monoclinic phase to relieve strain and subsequently transitions towards the high symmetry cubic configuration at elevated temperatures. There are three overarching linear volumetric thermal expansion regions (Fig. 9a) corresponding to (i) the region where the rhombohedral phase is dominant and the other phases are minimal, (ii) the region where there are drastic changes in the phase composition and (iii) the region where the cubic phase is dominant and only minor amounts of rhombohedral phase are present. This does not, however, reflect the complexity of the deformation of the unit cell due to expansion and contraction in the *a* and *c* directions. However, with lattice parameter *c* being approximately seven times that of *a* and larger changes occurring in the *c* direction, the *c* parameter dominates. Although the volume of the unit cell is different in the 3 regions, the rate of volumetric thermal expansion β_v is very similar throughout Fig. 9a.

For 2.5Y7.5LSB, a very similar behavior was observed with the same transformations taking place in very similar temperature ranges as seen in Fig. 10. However, at 656 °C, the material is only comprised of 79.4 % cubic phase, with the rhombohedral (18.1 %) and monoclinic (2.5 %) phases constituting the rest (Fig. 7f). This enables a more accurate determination of the cell parameters of the rhombohedral phase in the highest temperature range. Additionally, this emphasizes the combined effect of increased strain and higher dopant level increasing the stability

of lower symmetry phases and providing a stronger resistance towards cubic ordering. In this case, the cell parameters in region (iii) of Fig. 10a are similar to those in region (ii), but a slight deviation in the slope still results in three distinct regions with different rates of thermal expansion which are linked to the phases present.

The volumetric coefficients of thermal expansion β_v derived for 2Y5.5LSB and 2.5Y7.5LSB over 360–656 °C are comparable to the equivalent volumetric thermal expansion determined for cubic 22.5YSB over 589–769 °C [42]. The linear coefficient of thermal expansion α_l of δ-22.5YSB was found to be ~27.1×10^{-6} K^{-1} which can be approximated into a volumetric coefficient of thermal expansion β_v of ~81.3×10^{-6} K^{-1} (as described in Section 2.3 and in the Supplementary Information [31]). This similarity in the rate of volumetric thermal expansion is noteworthy and illustrates that while anisotropic thermal expansion was observed for the rhombohedral phases, the overall rate of volumetric thermal expansion is comparable to that of an analogous cubic bismuth oxide.

4. Conclusion

The phase stability window of rhombohedral doped Bi_2O_3 was investigated in terms of a wide range of dopant concentration (7.5–25 %) and weighted average cationic dopant radius (0.907–1.154 Å). Combining this work with that found in literature [15–17,20], it was seen that the rhombohedral phase could be stabilized in the lower dopant concentration range (~7.5–25 %) provided the average dopant radii is high enough (>~1.07 Å), and at slightly lower average dopant radii provided the dopant concentration is high enough (>~25 %), depending on the dopant identity. However, discrepancies were found in the regions (dopant concentration vs average dopant radii) where a pure rhombohedral phase was detected. These discrepancies indicate that the nature of the dopant cation and the synthetic methodology used both contribute significantly towards the stabilization of rhombohedral Bi_2O_3.

Investigating the *in situ* phase transformation behavior when heating rhombohedral-rich phase mixtures illustrated, for the first time, the complex phase transformations that occur and showed how these transformations are correlated to the anisotropic thermal expansion behavior of the rhombohedral phase. Although these transformations are undesirable in materials for SOFC applications, this study provides insight into mixed phase systems, be it as synthesized materials (as is the case here) or mixed phases from the degradation of a pure rhombohedral phase. For tetragonal plus rhombohedral-rich mixed phase materials with 7.5 % and 10 % total dopant concentration, partial transformation to an intermediate monoclinic polymorph was observed, which has not been reported before. This monoclinic phase formation precedes the formation of the cubic phase together with further rhombohedral-cubic phase transitions. Additionally, abrupt changes in the rhombohedral phase unit cell volume and separation of the (009) and (104) peaks of the rhombohedral phase at ~450 °C were found to be indicative of the β_2-to-β_1 rhombohedral phase transformation for both 2Y5.5LSB and 2.5Y7.5LSB. This transformation resulted in abrupt expansion and contraction in the *c* and *a* directions, respectively, and coincided with the formation of the monoclinic phase. The contraction in the *a* direction during the β_2-to-β_1 phase transformation is reported for the first time in this work and likely reflects the strain-relieving formation of the monoclinic phase. Additional anisotropic thermal expansion behavior over 500–656 °C was found to coincide with the various phase transitions which occur, such as the rhombohedral-cubic transformation which exhibits an onset temperature of ~550 °C. The overall anisotropic expansion behavior reflects a dynamic system where phase transformation and anisotropic expansion reflects the mitigation of strain by the system as it transitions towards the high order cubic phase. These results demonstrate that high La doping promotes stable rhombohedral phase formation, while lower dopant levels lead to undesirable phase transitions. To enhance phase stability under SOFC conditions, we propose that rhombohedral compositions should target high La substitution (≥17.5 %), maintain a high La:Y ratio, and minimize Al content to preserve a high average dopant cationic radius (≥1.10 Å).

CRediT authorship contribution statement

Mathias A. Kiefer: Writing – review & editing, Writing – original draft, Visualization, Validation, Software, Project administration, Methodology, Investigation, Formal analysis, Data curation, Conceptualization. **Caren Billing:** Writing – review & editing, Supervision, Resources, Project administration, Methodology, Funding acquisition, Formal analysis, Conceptualization. **Daniel Olds:** Writing – review & editing, Resources, Project administration, Investigation, Conceptualization. **David G. Billing:** Supervision, Resources, Project administration, Funding acquisition, Conceptualization.

Declaration of competing interest

The authors declare that they have no known competing financial interests or personal relationships that could have appeared to influence the work reported in this paper.

Acknowledgements

The authors acknowledge financial support for their research from the National Research Foundation (NRF, South Africa, Grant No: 141966) and Department of Science, Technology and Innovation (DSTI, South Africa, Grant UID: 41292), as well as the University of the Witwatersrand. This research used beamline 28-ID-1 of the National Synchrotron Light Source II, a U.S. Department of Energy (DOE) Office of Science User Facility operated for the DOE Office of Science by Brookhaven National Laboratory under Contract No. DE-SC0012704.

Appendix A. Supplementary data

Supplementary data to this article can be found online at https://doi.org/10.1016/j.jssc.2025.125597.

Data availability

Data will be made available on request.

References

[1] N.M. Sammes, G.A. Tompsett, H. Näfe, F. Aldinger, Bismuth based oxide electrolytes— structure and ionic conductivity, J. Eur. Ceram. Soc. 19 (1999) 1801–1826, https://doi.org/10.1016/S0955-2219(99)00009-6.
[2] P. Shuk, H.-D. Wiemhöfer, U. Guth, W. Göpel, M. Greenblatt, Oxide ion conducting solid electrolytes based on Bi_2O_3, Solid State Ionics 89 (1996) 179–196, https://doi.org/10.1016/0167-2738(96)00348-7.
[3] A.M. Azad, S. Larose, S.A. Akbar, Bismuth oxide-based solid electrolytes for fuel cells, J. Mater. Sci. 29 (1994) 4135–4151, https://doi.org/10.1007/BF00414192.
[4] E.M. Levin, R.S. Roth, Polymorphism of bismuth sesquioxide. I. Pure Bi_2O_3, J. Res. Natl. Bur. Stand. Sect. A Phys. Chem. 68A (2) (1964) 189–195, hmttps://doi.org/10.6028%2Fjres.068A.019.
[5] E.M. Levin, R.S. Roth, Polymorphism of bismuth sesquioxide. II. Effect of oxide additions on the polymorphism of Bi_2O_3, J. Res. Natl. Bur. Stand. Sect. A Phys. Chem. 68A (2) (1964) 197–206, hmttps://doi.org/10.6028%2Fjres.068A.020.
[6] P.D. Battle, C.R.A. Catlow, J.W. Heap, L.M. Moroney, Structural and dynamical studies of δ-Bi_2O_3 oxide ion conductors. I. The structure of $(Bi_2O_3)_{1-x}(Y_2O_3)_x$ as a function of *x* and temperature, J. Solid State Chem. 63 (1986) 8–15, https://doi.org/10.1016/0022-4596(86)90146-5.
[7] K.V. Kale, K.M. Jadhav, G.K. Bichile, Investigations on a high-conductivity solid electrolyte system, Bi_2O_3-Y_2O_3, J. Mater. Sci. Lett. 18 (1999) 9–11, https://doi.org/10.1023/A:1006652705028.
[8] T. Takahashi, H. Iwahara, T. Arao, High oxide ion conduction in sintered oxides of the system Bi_2O_3-Y_2O_3, J. Appl. Electrochem. 5 (1975) 187–195, https://doi.org/10.1007/BF01637268.
[9] C. Wang, X. Xu, B. Li, Ionic and electronic conduction of oxygen ion conductors in the Bi_2O_3-Y_2O_3 system, Solid State Ionics 13 (1984) 135–140, https://doi.org/10.1016/0167-2738(84)90047-X.
[10] J.G. Lee, S.H. Kim, H.H. Yoon, Synthesis of yttria-doped bismuth oxide powder by carbonate coprecipitation for IT-SOFC electrolyte, J. Nanosci. Nanotechnol. 11 (2011) 820–823, https://doi.org/10.1166/jnn.2011.3199.

[11] S.-F. Wang, Y.-F. Hsu, W.-C. Tsai, H.-C. Lu, The phase stability and electrical conductivity of Bi_2O_3 ceramics stabilized by Co-dopants, J. Power Sources 218 (2012) 106–112, https://doi.org/10.1016/j.jpowsour.2012.06.056.
[12] X.J. Zhang, W.T. Jin, S.J. Hao, Y. Zhao, H. Zhang, Study of the crystal structures of new buffer materials $Bi_{1-x}Y_xO_{1.5}$, J. Supercond. Nov. Magnetism 23 (2010) 1011–1014, https://doi.org/10.1007/s10948-009-0615-1.
[13] Y.-C. Wu, Y.-W. Chang, S.-F. Wang, Electrical properties and microstructural analysis of aliovalent-ion (Y^{3+}, Nb^{5+})–Doped bismuth-based solid-oxide electrolyte, Ferroelectrics 455 (2013) 123–128, https://doi.org/10.1080/00150193.2013.845486.
[14] A. Watanabe, T. Kikuchi, Cubic-hexagonal transformation of yttria-stabilized δ-bismuth sesquioxide, $Bi_{2-2x}Y_{2x}O_3$ (x=0.215-0.235), Solid State Ionics 21 (1986) 287–291, https://doi.org/10.1016/0167-2738%2886%2990191-8.
[15] A.G. Jolley, R. Jayathilake, E.D. Wachsman, Optimizing rhombohedral Bi_2O_3 conductivity for low temperature SOFC electrolytes, Ionics 25 (2019) 3531–3536, https://doi.org/10.1007/s11581-019-02920-x.
[16] T. Takahashi, H. Iwahara, Y. Nagai, High oxide ion conduction in sintered Bi_2O_3 containing SrO, CaO or La_2O_3, J. Appl. Electrochem. 2 (1972) 97–104, https://doi.org/10.1007/BF00609125.
[17] H. Iwahara, T. Esaka, T. Sato, T. Takahashi, Formation of high oxide ion conductive phases in the sintered oxides of the system Bi_2O_3-Ln_2O_3 (Ln = La-Yb), J. Solid State Chem. 39 (1981) 173–180, https://doi.org/10.1016/0022-4596(81)90328-5.
[18] M. Drache, S. Obbade, J.P. Wignacourt, P. Conflant, Structural and conductivity properties of $Bi_{0.775}Ln_{0.225}O_{1.5}$ oxide conductors (ln = La, Pr, Nd, Sm, Eu, Gd, Tb, dy) with rhombohedral Bi-Sr-O type, J. Solid State Chem. 142 (1999) 349–359, https://doi.org/10.1006/jssc.1998.8043.
[19] A.G. Jolley, Q. Bai, R. Jayathilake, Y. Mo, E.D. Wachsman, Bismuth oxide electrolytes with superior conductivity and stability, Mater. Today 86 (2025) 247–254, https://doi.org/10.1016/j.mattod.2025.03.030.
[20] D. Mercurio, M. El Farissi, B. Frit, J.M. Reau, J. Senegas, Fast ionic conduction in new oxide materials of the Bi_2O_3-Ln_2O_3-TeO_2 systems (Ln=La, Sm, Gd, Er), Solid State Ionics 39 (1990) 297–304, https://doi.org/10.1016/0167-2738(90)90410-S.
[21] A.E. Danks, S.R. Hall, Z. Schnepp, The evolution of 'sol-gel' chemistry as a technique for materials synthesis, Mater. Horiz. 3 (2016) 91–112, https://doi.org/10.1039/C5MH00260E.
[22] X. Shi, S. Ghose, E. Dooryhee, Performance calculations of the X-ray powder diffraction beamline at NSLS-II, J. Synchrotron Radiat. 20 (2013) 234–242, https://doi.org/10.1107/S0909049512049175.
[23] D.L. Kaiser, R.L. Watters, SRM 640d - Silicon Powder - Line Position and Line Shape Standard for Powder Diffraction, vols. 1–5, National Institute of Standards and Technology, 2010. Available at: https://www-s.nist.gov/srmors/certificates/archives/640d.pdf. (Accessed 2 January 2021).
[24] K.G. Lyon, G.L. Salinger, C.A. Swenson, G.K. White, Linear thermal expansion measurements on silicon from 6 to 340 K, J. Appl. Phys. 48 (1977) 865–868, https://doi.org/10.1063/1.323747.
[25] Y. Okada, Y. Tokumaru, Precise determination of lattice parameter and thermal expansion coefficient of silicon between 300 and 1500 K, J. Appl. Phys. 56 (1984) 314–320, https://doi.org/10.1063/1.333965.
[26] A.A. Coelho, TOPAS and TOPAS-Academic: An optimization program integrating computer algebra and crystallographic objects written in C++, J. Appl. Crystallogr. 51 (2018) 210–218. https://doi.org/10.1107/S1600576718000183.
[27] R.E. Dinnebier, A. Leineweber, J.S.O. Evans (Eds.), Rietveld Refinement Practical Powder Diffraction Pattern Analysis Using Topas, first ed. vol. 1, Walter de Gruyter GmbH, Berlin/Boston, 2019, pp. 16–129.
[28] R.W. Cheary, A.A. Coelho, J.P. Cline, Fundamental parameters line profile fitting in laboratory diffractometers, J. Res. Natl. Inst. Stand. Technol. 109 (1) (2004) 1–25, https://doi.org/10.6028/jres.109.002.
[29] R.W. Cheary, A.A. Coelho, Axial divergence in a conventional X-ray powder diffractometer. I. Theoretical foundations, J. Appl. Crystallogr. 31 (1) (1998) 851–861, https://doi.org/10.1107/S0021889898006876.
[30] P. Thompson, D.E. Cox, J.B. Hastings, Rietveld refinement of debye-scherrer synchrotron X-ray data from Al_2O_3, J. Appl. Crystallogr. 20 (1) (1987) 79–83, https://doi.org/10.1107/S0021889887087090.
[31] V.A. Drebushchak, Thermal expansion of solids: review on theories, J. Therm. Anal. Calorim. 142 (2020) 1097–1113, https://doi.org/10.1007/s10973-020-09370-y.
[32] R.D. Shannon, Revised effective ionic radii and systematic studies of interatomic distances in halides and chalcogenides, Acta Crystallogr. 32 (1976) 751–767, https://doi.org/10.1107/S0567739476001551.
[33] M. Thrall, R. Freer, C. Martin, F. Azough, B. Patterson, R.J. Cernik, An in situ study of the formation of multiferroic bismuth ferrite using high resolution synchrotron X-ray powder diffraction, J. Eur. Ceram. Soc. 28 (2008) 2567–2572, https://doi.org/10.1016/j.jeurceramsoc.2008.03.029.
[34] M. Struzik, M. Malys, M. Krynski, M. Wojcik, J.R. Dygas, W. Wrobel, F. Krok, I. Abrahams, Structural and electrical behaviour in $Bi_{14}YO_{22.5}$, RSC Adv. 5 (2015) 83471–83479, https://doi.org/10.1039/c5ra18709e.
[35] A. Borowska-Centkowska, X. Liu, M. Krynski, M. Leszczynska, W. Wrobel, M. Malys, S. Hull, S.T. Norberg, F. Krok, I. Abrahams, Defect structure in δ-$Bi_5PbY_2O_{11.5}$, RSC Adv. 9 (2019) 9640–9653, https://doi.org/10.1039/C9RA01233H.
[36] E.A. Payzant, W.D. Porter, C.R. Hubbard, High temperature phase transformation in rhombohedral bismuth strontium oxide, Thermochim. Acta 318 (1998) 45–50, https://doi.org/10.1016/S0040-6031(98)00328-1.
[37] D. Mercurio, J.C. Champarnaud-Mesjard, B. Frit, P. Conflant, J.C. Boivin, T. Vogt, Thermal evolution of the single crystal structure of the rhombohedral $Bi_{0.75}Sr_{0.25}O_{1.375}$ phase: a single crystal neutron diffraction study, J. Solid State Chem. 112 (1994) 1–8, https://doi.org/10.1006/jssc.1994.1255.
[38] E.A. Payzant, H.W. King, A high temperature X-Ray diffraction investigation of the β-$(Bi_2O_3)_{1-x}(SrO)_x$ solid solution, Can. Metall. Q. 41 (2) (2002) 263–272, https://doi.org/10.1179/cmq.2002.41.2.263.
[39] P. Conflant, J.C. Boivin, D. Thomas, Le Diagramme des Phases Solides du Systeme Bi_2O_3-CaO, J. Solid State Chem. 18 (1976) 133–140, https://doi.org/10.1016/0022-4596(76)90087-6.
[40] P. Conflant, J.C. Boivin, D. Nowgrocki, D. Thomas, Etude structural par diffractometrie x a haute temperature du conducteur anionique $Bi_{0,844}Ba_{0,156}O_{1,422}$, Solid State Ionics 9&10 (1983) 925–928, https://doi.org/10.1016/0167-2738(83)90112-1.
[41] J.C. Boivin, D.J. Thomas, Crystal chemistry and electrical properties of bismuth-based mixed oxides, Solid state ion 5 (1981) 523–526, https://doi.org/10.1016/0167-2738(81)90307-6.
[42] M.A. Kiefer, C. Billing, R.M. Erasmus, W.M. Mogodi, D.G. Billing, A detailed investigation of the structural stability, ionic conductivity and in situ δ-phase formation of $Y_xBi_{2-x}O_δ$, S. Afr. J. Chem. 76 (2022) 111–119, https://doi.org/10.17159/0379-4350/2022/v76a16.